ACSNANO

www.acsnano.org

ARTICLE

Bimodal Tactile Sensor without Signal Fusion for User-Interactive Applications

Xiaole Ma, Chunfeng Wang,* Ruilai Wei, Jiaqi He, Jing Li, Xianhu Liu, Fengchang Huang, Shuaipeng Ge, Juan Tao, Zuqing Yuan, Ping Chen, Dengfeng Peng, and Caofeng Pan*

Cite This: *ACS Nano* 2022, 16, 2789−2797

Read Online

ACCESS | Metrics & More | Article Recommendations | Supporting Information

ABSTRACT: **Tactile sensors with multimode sensing ability are cornerstones of artificial skin for applications in humanoid robotics and smart prosthetics. However, the intuitive and interference-free reading of multiple tactile signals without involving complex algorithms and calculations remains a challenge. Herein a pressure−temperature bimodal tactile sensor without any interference is demonstrated by combining the fundamentally different sensing mechanisms of optics and electronics, enabling the simultaneous and independent sensing of pressure and temperature with the elimination of signal separation algorithms and calculations. The bimodal sensor comprises a mechanoluminescent hybrid of ZnS−CaZnOS and a poly(3,4-ethylenedioxythiophene):poly(styrene sulfonate) (PEDOT:PSS) thermoresistant material, endowing the unambiguous transduction of pressure and temperature into optical and electrical signals, respectively. This device exhibits the highest temperature sensitivity of −0.6% °C^{-1} in the range of 21−60 °C and visual sensing of the applied forces at a low limitation of 2 N. The interference-free and light-emitting characteristics of this device permit user-interactive applications in robotics for encrypted communication as well as temperature and pressure monitoring, along with wireless signal transmission. This work provides an unexplored solution to signal interference of multimodal tactile sensors, which can be extended to other multifunctional sensing devices.**

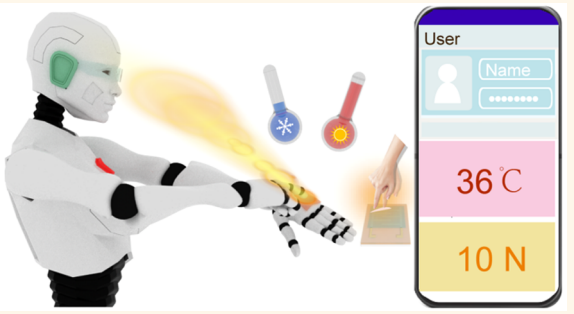

KEYWORDS: *tactile sensor, multimode sensing, hybrid mechanism, humanoid robotics, smart prosthetics*

INTRODUCTION

Human skin, comprising an integrated network of sensory receptors, relays information on mechanical and thermal stimuli to the brain, allowing us to maneuver within the surrounding environment effectively and safely. Mimicry of the human skin represents an emerging and promising direction toward the implementation of humanoid robotics, biomimetic prosthetics, and artificial intelligence.[1−14] In the last decades, many endeavors have been dedicated to augmenting artificial skin with mechanical and thermal sensing abilities, with emphasis on the development of multifunctional materials responsive to multiple stimuli or the arranged integration of various sensory units into a hybrid system.[15−25] For example, organic semiconductors combined with a transistor[26,27] or capacitor structure[28] were identified for a large-scale matrix of pressure and thermal sensors; carbon nanomaterials (carbon nanotubes, graphene, *etc.*) with forms of yarn,[29,30] sponge,[31−34] and microstructures[35−37] were developed for flexible sensing of pressure and temperature; metal percolation or mesh was patterned into a transparent panel with pressure and temperature sensing;[38,39] ferroelectric composites with a designed interlock construction demonstrated the enhanced or self-powered sensing of pressure and temperature;[40−42] hydrogels with conductive fillers were proposed for self-healing and sensing of pressure and temperature;[43,44] and individual pressure and temperature sensory pixels connected with serpentine electrodes were applied to create a stretchable array for multifunctional sensing.[45] Despite the thriving progress, these bimodal sensors produce signals responsive to temperature and pressure that are similar, such as relative changes in resistance, capacitance, voltage, or current. These signals are often fused, thereby hampering their application in real-time monitoring of temperature and pressure with the necessary discrimination, and thus, a follow-up signal separation algorithm or calculation is required. A recent study achieved differentiation of pressure and temperature

Received: November 4, 2021
Accepted: January 11, 2022
Published: January 21, 2022

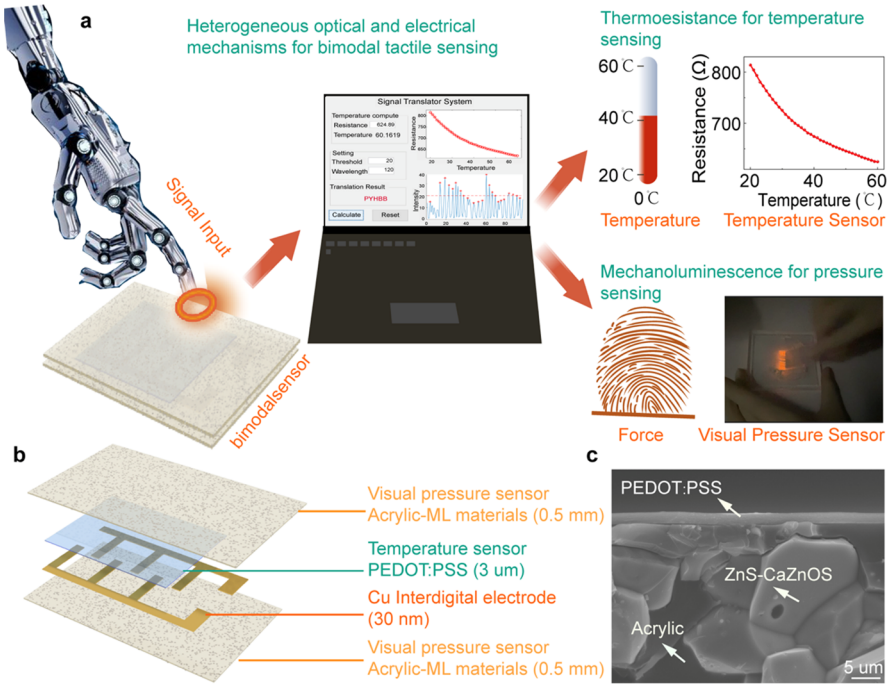

Figure 1. Heterogeneous optical and electrical mechanisms for pressure and temperature sensing. (a) Concept of combining heterogeneous sensing mechanisms of mechanoluminescence and thermoresistance for bimodal tactile sensing and related applications such as a visible user−robotic interaction. (b) Schematic structure of the bimodal tactile senor. (c) Cross-sectional SEM image of the bimodal tactile sensor, showing the pressure-sensing layer of the ZnS−CaZnOS ML hybrids and the PEDOT:PSS thermal-sensing layer.

based on ion relaxation dynamics, with an additional variable of the charge relaxation time as a strain-insensitive intrinsic variable to measure absolute temperature.[46] This work inspires signal decoupling by introducing additional variables that are fundamentally different from the original ones.

Herein we present an interference-free bimodal tactile sensor for pressure and temperature sensing through the conjunction of fundamentally different variables of resistance and luminescence. The heterogeneity of the optical and electrical mechanisms within this device enables the sensing of pressure and temperature independently and expediently without any crosstalk. The pressure is visually identified by the piezo/tribophotonic effect of ZnS−CaZnOS mechanoluminescent (ML) hybrids, and the temperature sensing is realized by the thermoresistive effect of PEDOT:PSS. The device exhibits a temperature sensitivity of −0.6% $°C^{-1}$ in the range of 21−60 °C and can visually sense applied forces with a low detection limit of 2 N. More importantly, the signal-self-differentiation and light-emitting features of the device not only guarantee a visual user−robotic interaction but also allow wireless sensory feedback of pressure and temperature with the developed application in mobile phones.

RESULTS AND DISCUSSION

Heterogeneous Optical and Electrical Mechanisms for Bimodal Sensing. The key idea of this work is presented in Figure 1a, where a combination of heterogeneous sensing mechanisms of mechanoluminescence and thermoresistance are proposed for bimodal sensing and related applications. The structure of the bimodal sensor is hierarchically illustrated in Figure 1b, in which the temperature sensor composed of a PEDOT:PSS film and copper interdigital electrode is sandwiched between two luminescent layers with ML hybrids embedded in the acrylic polymer (see Materials and Methods and Figure S1 for fabrication details). The temperature-sensing layer has a thin profile with a PEDOT:PSS thickness of approximately 3 μm and a negligible thickness of the copper electrode, as shown in Figures 1c and S2. This temperature-sensing layer is much thinner than the luminescent layers, each with a thickness of approximately 0.5 mm, and therefore, an approximately neutral mechanical region may occur in the temperature-sensing layer, contributing to effective strain decoupling as well.

Single-Mode Pressure Sensing by ML Hybrids. ML materials that directly convert mechanical stimuli into light have been emerging in optical pressure sensors with the advancement of self-powered, wireless, and visual sensing.[47−54] In this work, a high-performance ML hybrid was synthesized and developed for the visual sensing and imaging of pressure (see Materials and Methods for synthetic details). The ML hybrids are composed of a ZnS phase and a CaZnOS phase doped with the transition metal element manganese. They have a mean size of approximately 7 μm (Figure S3) and can emit bright and vivid light under multiple mechanical stimuli (Video S1). The biphasic feature is identified by the X-ray diffraction (XRD) pattern in Figure 2a, where the diffraction peaks are indexed with either standard ZnS or standard CaZnOS. The biphasic characteristic enhances the ML emission as a result of the improved carrier transfer and recombination induced by the band offset between ZnS and CaZnOS at the interface.[55] Figure 2b presents energy-dispersive X-ray spectroscopy (EDS) mapping images of a representative ML hybrid particle, which reveal the presence of the Mn dopant in both the ZnS and CaZnOS phases, leading to two different delay lifetimes upon excitation at 295 nm with the monitored emission wavelengths of 590 and 620 nm, respectively (Figure 2c). These results indicate that both ZnS:Mn and CaZnOS:Mn exist in the ML hybrids and

https://doi.org/10.1021/acsnano.1c09779
ACS Nano 2022, 16, 2789−2797

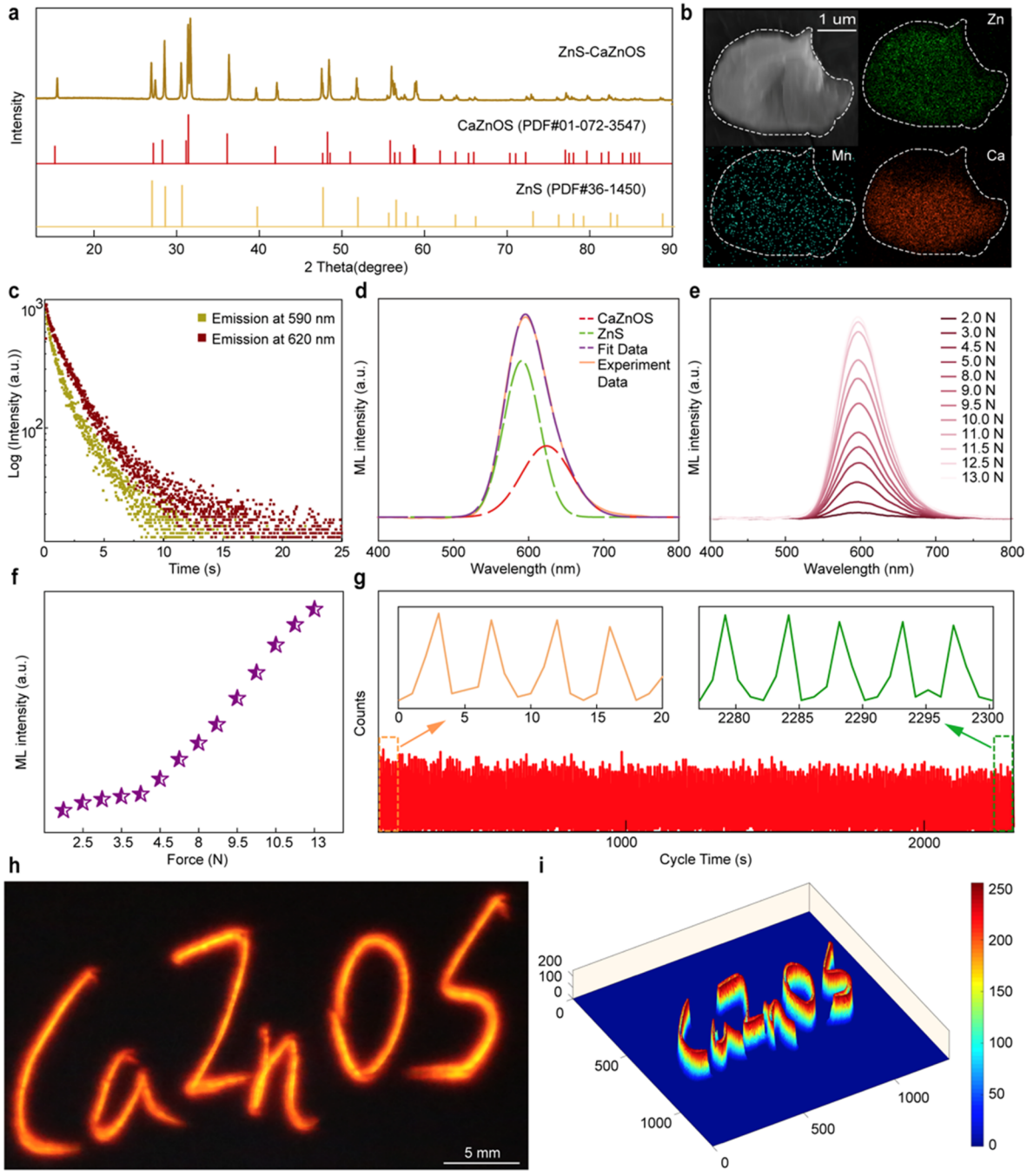

Figure 2. Single-mode pressure sensing by ML hybrids. (a) XRD pattern of the ML hybrids composed of a ZnS phase and a CaZnOS phase. (b) EDS mapping images of a representative ML particle. (c) Transient photoluminescence decay curves of the ML hybrids. (d) Peak deconvolution of the ML spectrum with Gaussian functions. (e) ML spectra of the as-fabricated pressure sensor at various applied forces. (f) Light-emission intensities of the pressure sensor under the different forces, extracted from (e) at the wavelength of 596 nm. (g) Cycling stability of the pressure sensor. (h) Visual sensing of the dynamic force applied to the pressure sensor and (i) the corresponding three-dimensional intensity profile extracted by a self-developed program.

simultaneously contribute to the final light emission, as shown by the deconvolution of the ML spectrum (Figure 2d).

The ML spectra of the as-fabricated pressure sensor in response to different forces are shown in Figure 2e. The sensor can illuminate at a small force of 2 N (corresponding to a pressure of 4 MPa), and the ML intensity increases as the force increases, while the emission peak remains consistent at approximately 596 nm. The ML intensity shows a nonlinear relationship with the applied forces (Figure 2f), which can be ascribed to the piezo/tribophotonic effect of the ML hybrids composed of piezoluminescence and triboluminescence. Figure 2g shows the cycling stability of the pressure sensor, demonstrating stable ML performance over 2300 cycles. The ML attribute of the pressure sensor permits self-powered and visual sensing and imaging of the applied force, as shown in Figure 2h. Here, the force generates vivid light that can be observed by the naked eye or recorded by a camera, and the affiliated information on the force, such as amplitude and trajectory, can be determined by the corresponding three-

https://doi.org/10.1021/acsnano.1c09779
ACS Nano 2022, 16, 2789−2797

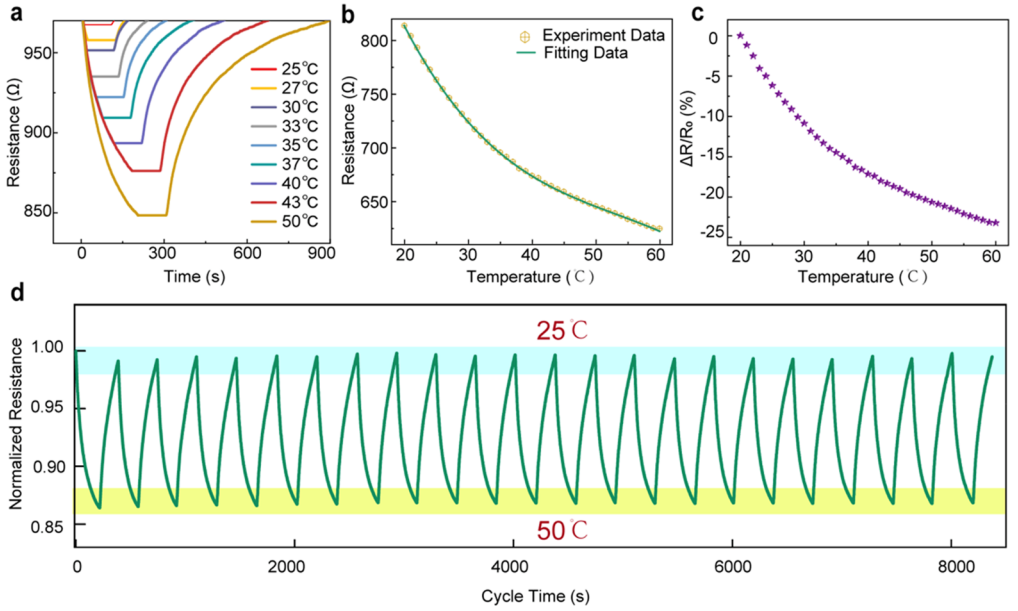

Figure 3. Single-mode thermal sensing by PEDOT:PSS. (a) Response curves of the temperature sensor to different temperatures. (b) Dependence of the resistance on the temperature of the temperature sensor along with the calibration. (c) Relative resistance change vs temperature, indicating the sensitivity of the temperature sensor. (d) Normalized relative resistance variation during the heating and cooling process.

dimensional intensity profile extracted by a self-developed program (Figure 2i).

Single-Mode Thermal Sensing by PEDOT:PSS. PEDOT:PSS was selected for the fabrication of the temperature sensor because of its favorable electrical and mechanical properties. The temperature-dependent behavior of PEDOT:PSS originates from the thermoresistive effect, where the carrier mobility rate of PEDOT:PSS increases as the temperature increases, leading to a decrease in the resistance of PEDOT:PSS at elevated temperatures,[56] as indicated by the temperature-responsive curve of the temperature sensor in Figure 3a. The relationship between the resistance (Y) and temperature (X) of the temperature sensor is shown in Figure 3b and can be calibrated using the ternary equation $Y = 1177.37675 - 25.97355X + 0.44683X^2 - 0.0028X^3$ with a determination coefficient (R^2) of 0.99983. The high determination coefficient indicates an excellent correlation between the resistance and temperature of the temperature sensor. The relative resistance change $\Delta R = \frac{R - R_0}{R_0}$ (where R_0 and R are the resistances at 20 °C and from 21 to 60 °C, respectively) as a function of temperature is shown in Figure 3c, from which the sensitivity of the temperature sensor can be extracted with a value of −0.6% °C^{-1}. Figure 3d shows the stability and reliability of the temperature sensor following cyclic heating (50 °C) and cooling (25 °C) sequences, where the normalized resistance change remained consistent over multiple heating/cooling cycles, showing durable operation of the temperature sensor.

Bimodal Pressure−Temperature Sensing. The setup for the bimodal sensing test is schematically shown in Figures 4a and S4. The sample temperature is controlled by a Peltier component connected to the DC generator, and the force is applied to the sample by a linear motor with a dynamometer for quantification. The sensing signals responsive to temperature and pressure were simultaneously collected and recorded using an LCR meter and an optical spectrometer, respectively. Figure 4b presents the temperature responses of the bimodal sensor at 40 °C with different applied forces, in which the thermal response curves exhibit a coincident profile over the changed forces, indicating the pressure insensitivity of the bimodal sensor during temperature sensing. The influence of temperature on the pressure response of the bimodal sensor is shown in Figure 4c, in which the ML spectra at a force of 6 N overlap well with the temperature changes, showing the temperature insensitivity of the bimodal sensor during pressure sensing within the tested temperature range. In addition, simultaneous and independent sensing of pressure and temperature by the bimodal sensor was investigated, as shown in Figure 4d, where the optical and electrical sensing signals remained consistent under the continuously changing stimuli of pressure and temperature, proving the interference-free sensing ability of the bimodal sensor.

Bimodal Sensor for User-Interactive Applications. A user-interactive interface with sensory feedback is significant for humanoid robots to perceive external stimuli and simultaneously exchange information with humans. Our devices with bimodal sensing and light-emitting features permit their application as user-interactive interfaces for robotics that not only realize the perception of external stimuli of temperature and pressure but also enable the conversion of pressure into encrypted information that can be recognized by robots and is visible to humans, as illustrated in Figure 5a. The information conversion is based on the quantitative relationship between pressure and ML intensity, wherein the ML intensity signals can be binarily determined as "0" or "1" using a translation program with a selected threshold. Figure 5b demonstrates the representative conversion of ML signals into the letter "B", with corresponding binary data of [0, 0, 0, 0, 1]. A series of letters and numbers can be determined using this binary cipher (Table S1 and Figure S5), endowing the acquisition of words, phrases, and sentences with the encrypted information for communication between humans and robots. Meanwhile, the pressure can be visible to the human eye,

https://doi.org/10.1021/acsnano.1c09779
ACS Nano 2022, 16, 2789−2797

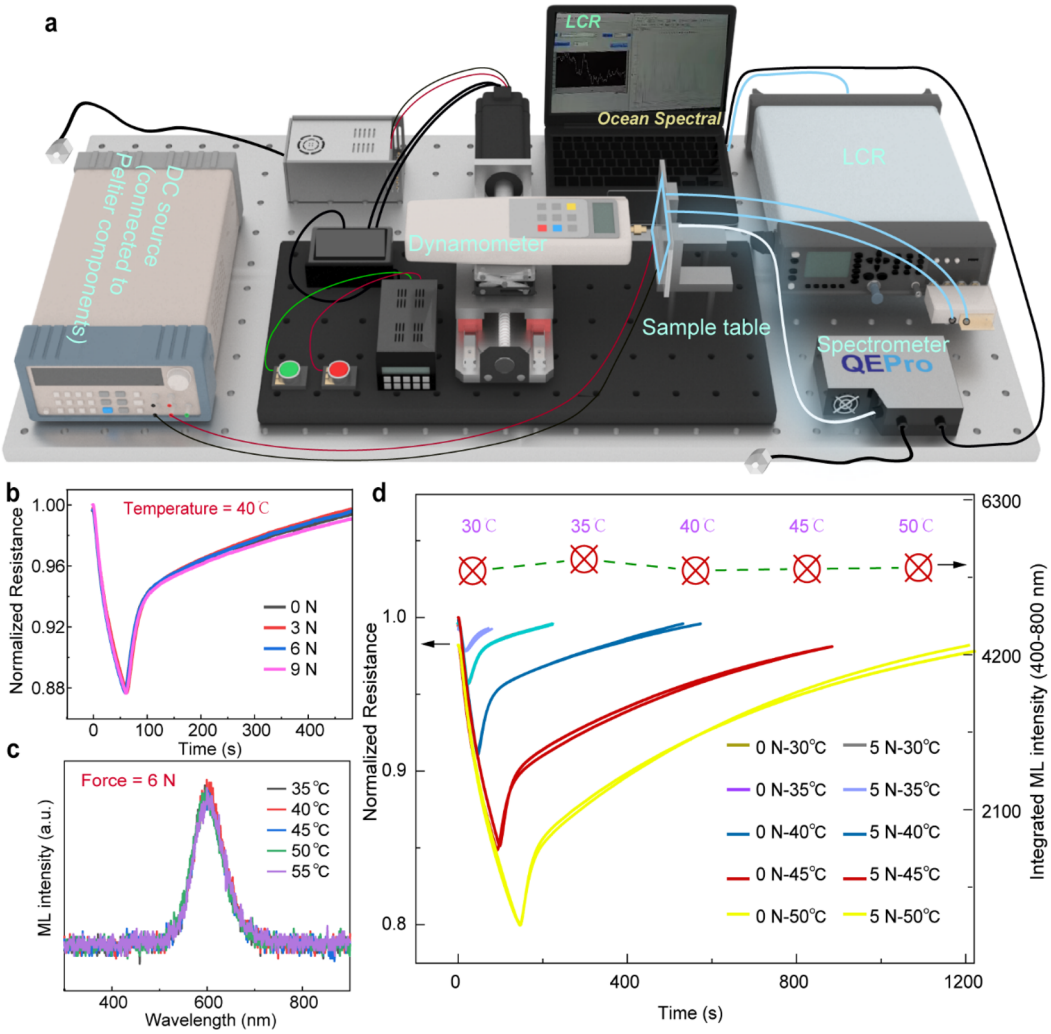

Figure 4. Bimodal sensing performance. (a) Schematic of the setup for the bimodal sensing test. (b) Temperature response curves of the bimodal sensor at 40 °C at different applied forces, indicating the pressure insensitivity of the device during temperature sensing. (c) ML spectra of the bimodal sensor under a force of 6 N at different temperatures, showing the temperature insensitivity of the device during pressure sensing. (d) Simultaneous and independent sensing of pressure and temperature of the bimodal sensor with continuously changing pressure and temperature stimuli.

impressing the human−robot interaction. The simultaneous information conversion and temperature sensing are demonstrated as well, as shown in Figure 5c and Video S2, in which the object temperature and force-delivered information on "BINN" can be recognized unambiguously.

Remote interaction and monitoring are also desired for active user-interactive systems. We demonstrated the wireless transmission of sensory data from our user-interactive device to a smartphone using a custom-developed application. The conceptual representation of wireless data transmission is shown in Figures 5d and S6, where the sensing information is first collected and uploaded to the cloud and then extracted and displayed by the developed application. The results of remote interaction and monitoring are depicted in Figure 5e and Videos S3 and S4, where the force-delivered information and the sensing signals of temperature and pressure can be read remotely and simultaneously, enabling convenient interaction between wearers and supervisors. This process also holds immense potential in wireless health-monitoring systems.

CONCLUSIONS

We have demonstrated a bimodal sensor of temperature and pressure without signal fusion for tactile sensing and user-interactive applications. The combined sensing mechanisms of piezo/tribophotonic and thermoresistive effects enable the independent transduction of mechanical and thermal stimuli into optical and electrical signals, respectively, with a temperature sensitivity of −0.6% $°C^{-1}$ and a force detection limitation of 2 N. The perception of external stimuli and the conversion of pressure into encrypted communication information for humanoid robots were demonstrated. A wireless sensory system was developed for remote information interaction and health monitoring. This work inspires dedication to multimodal sensors composed of multiple heterogeneous mechanisms for extended sensing and applications.

MATERIALS AND METHODS

Materials. $CaCO_3$ (99.99%, Alfa-Aesar), ZnS (99.99%, Aladdin), $MnCO_3$ (>99.99%, Sigma-Aldrich), acrylic, and PEDOT:PSS (Sigma-Aldrich) were all purchased and used as received.

https://doi.org/10.1021/acsnano.1c09779
ACS Nano 2022, 16, 2789−2797

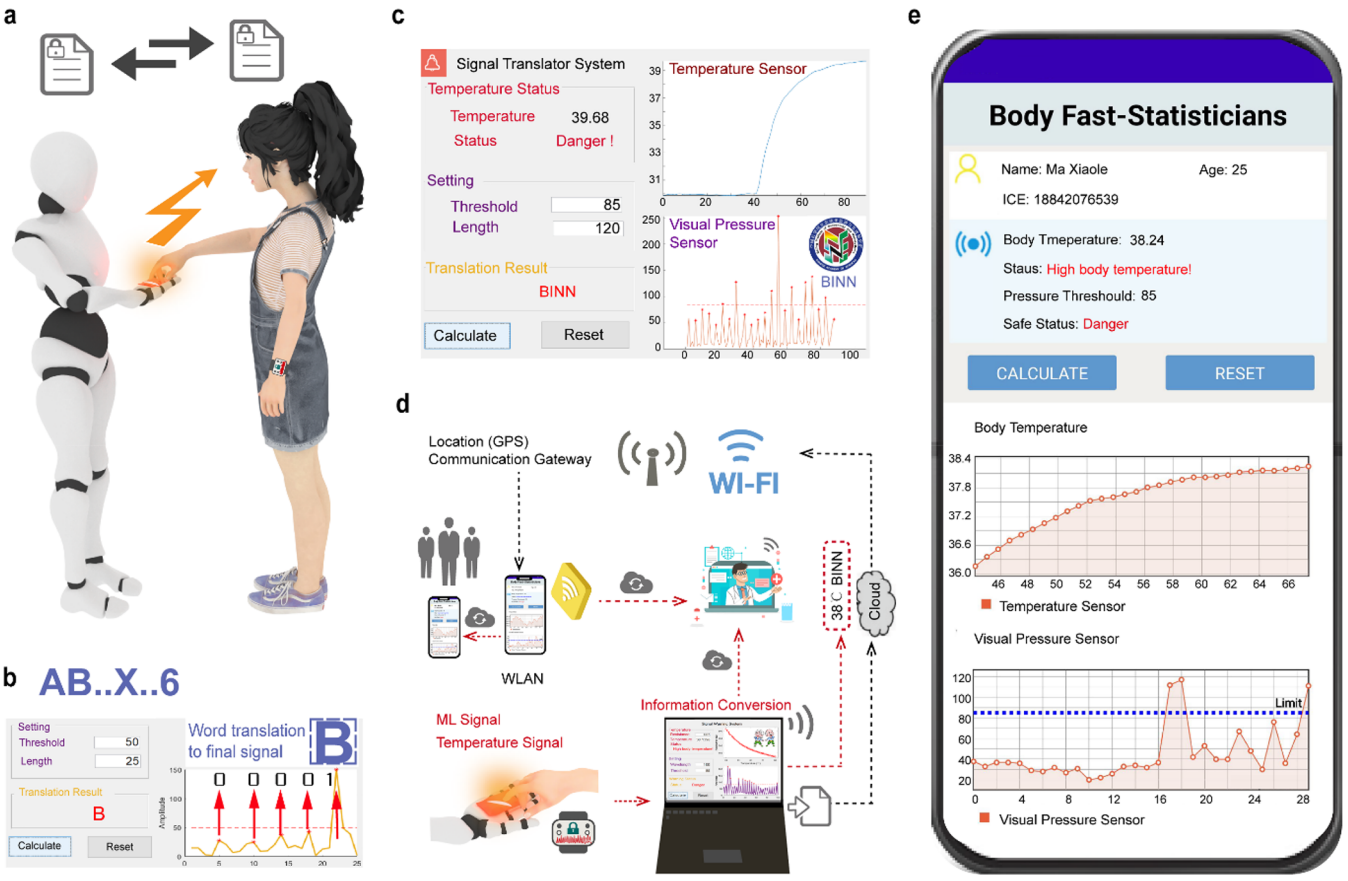

Figure 5. Bimodal sensor for user-interactive applications. (a) Concept of the bimodal sensor as user-interactive interface of robotics for the perception of external stimuli of temperature and pressure and simultaneously the conversion of pressure into encrypted information that can be recognized by robotics and visible to humans. (b) Conversion of ML signals into the letter "B", with corresponding binary data of [0, 0, 0, 0, 1]. (c) Simultaneous information conversion and temperature sensing. (d) Schematic diagram of wireless data transmission for remote interaction. (e) Remote monitoring of temperature and pressure *via* the custom-developed application on a smartphone.

Synthesis of ZnS−CaZnOS ML Hybrids. The ZnS−CaZnOS ML hybrids were prepared *via* a conventional high-temperature solid-state reaction, as reported in our previous work.[55] The raw materials of $CaCO_3$, ZnS, and $MnCO_3$ were weighed with a Ca:Zn:Mn molar ratio of 1:2:0.01 and mixed evenly in an agate mortar assisted with ethanol (until the ethanol was almost volatilized). The mixture was transferred into a corundum boat and desiccated at 80 °C for 4 h in an oven, followed by calcination at 1100 °C for 4 h in a horizontal tube furnace under an 80 sccm argon atmosphere. The entire calcination program included heating the sample from room temperature (~20 °C) to 800 °C with a temperature rise rate of 10 °C/min, keeping the temperature steady at 800 °C for 1 h, raising the temperature from 800 to 1100 °C at a rate of 5 °C/min, maintaining the temperature at 1100 °C for 4 h, and stopping the heating program. The product was naturally cooled to room temperature and ground into fine powder in a ball mill for use.

Fabrication of the Bimodal Tactile Sensor. The process for fabrication of the bimodal tactile sensor is shown schematically in Figure S1. The composite composed of the ML hybrid and acrylic precursor with a weight ratio of 7:3 was mixed uniformly, poured into a silicone mold, and then desiccated at 60 °C for 4 h in an oven. The composite layer was peeled off from the silicone mold for copper electrode deposition of the temperature sensor *via* the sputtering method with an interdigital shadow mask for electrode patterning. The thermoresistive layer of PEDOT:PSS was spin-coated onto the interdigital copper electrode at 300 rpm for 30 s and then cured at 50 °C for 1 h in an oven. The obtained product was placed into the silicone mold again and coated with another layer of ML−acrylic composite by repeating the previous steps. The bimodal sensor has a hierarchical structure with a thermal sensing layer sandwiched by pressure-sensing layers. An approximately neutral mechanical region may occur in the temperature-sensing layer owing to the designed thickness of each layer (PEDOT:PSS = 3 μm, Cu = 30 nm, ML-acrylic = 0.5 mm).

Characterizations. The structure of the ML hybrid was characterized using XRD. The morphology and elemental composition of the ML hybrids were characterized using field-emission scanning electron microscopy (SEM) (FEI Nova NanoSEM 450 microscope) equipped with an EDS accessory. The photoluminescence transient decay lifetime was measured using a fluorescence spectrometer (Edinburgh FLS 1000). The ML performance was measured using a homemade setup composed of a linear motor, force dynamometer, and fiber optic spectrometer (Ocean Optics QE65pro).

The sensing performance of the bimodal tactile sensor was characterized using a homemade setup, as shown in Figure S4. The sample temperature was controlled by a Peltier component connected to the DC generator. The force was applied to the sample by a linear motor with a dynamometer for quantization. The sensing signals responsive to temperature and pressure were simultaneously collected and recorded using an LCR meter (Agilent E4980A) and an optical spectrometer, respectively.

ASSOCIATED CONTENT

Supporting Information

The Supporting Information is available free of charge at https://pubs.acs.org/doi/10.1021/acsnano.1c09779.

Fabrication process of the dual-modal sensor (Figure S1); SEM images of PEDOT:PSS (Figure S2) and ML

https://doi.org/10.1021/acsnano.1c09779
ACS Nano 2022, 16, 2789−2797

materials (Figure S3); setup of bimodal sensing measurement (Figure S4); results of encrypted communication and temperature and pressure monitoring (Figure S5 and Table S1); flowchart of data transmission for wired and wireless displays (Figure S6) (PDF)

Light emission of the ML hybrids under different mechanical stimuli (Video S1); simultaneous information conversion and temperature sensing using the developed MATLAB GUI program (Video S2); remote monitoring of temperature and pressure using the developed application on a mobile phone (Video S3); remote encryption communication and temperature sensing using the developed application on a mobile phone (Video S4) (ZIP)

AUTHOR INFORMATION

Corresponding Authors

Caofeng Pan − *Center on Nanoenergy Research, School of Physical Science and Technology, Guangxi University, Nanning, Guangxi 530004, P. R. China; CAS Center for Excellence in Nanoscience, Beijing Key Laboratory of Micro-Nano Energy and Sensor, Beijing Institute of Nanoenergy and Nanosystems, Chinese Academy of Sciences, Beijing 101400, P. R. China; School of Nanoscience and Technology, University of Chinese Academy of Sciences, Beijing 100049, P. R. China;* orcid.org/0000-0001-6327-9692; Email: cfpan@binn.cas.cn

Chunfeng Wang − *Key Laboratory of Optoelectronic Devices and Systems of the Ministry of Education and Guangdong Province, College of Physics and Optoelectronic Engineering, Shenzhen University, Shenzhen 518060, P. R. China*; Email: cfwang@szu.edu.cn

Authors

Xiaole Ma − *Center on Nanoenergy Research, School of Physical Science and Technology, Guangxi University, Nanning, Guangxi 530004, P. R. China; CAS Center for Excellence in Nanoscience, Beijing Key Laboratory of Micro-Nano Energy and Sensor, Beijing Institute of Nanoenergy and Nanosystems, Chinese Academy of Sciences, Beijing 101400, P. R. China*

Ruilai Wei − *Center on Nanoenergy Research, School of Physical Science and Technology, Guangxi University, Nanning, Guangxi 530004, P. R. China*

Jiaqi He − *CAS Center for Excellence in Nanoscience, Beijing Key Laboratory of Micro-Nano Energy and Sensor, Beijing Institute of Nanoenergy and Nanosystems, Chinese Academy of Sciences, Beijing 101400, P. R. China*

Jing Li − *Center on Nanoenergy Research, School of Physical Science and Technology, Guangxi University, Nanning, Guangxi 530004, P. R. China*

Xianhu Liu − *National Engineering Research Center for Advanced Polymer Processing Technology, Zhengzhou University, Zhengzhou 450002, P. R. China;* orcid.org/0000-0002-4975-3586

Fengchang Huang − *Center on Nanoenergy Research, School of Physical Science and Technology, Guangxi University, Nanning, Guangxi 530004, P. R. China*

Shuaipeng Ge − *Key Laboratory of Optoelectronic Devices and Systems of the Ministry of Education and Guangdong Province, College of Physics and Optoelectronic Engineering, Shenzhen University, Shenzhen 518060, P. R. China*

Juan Tao − *Key Laboratory of Optoelectronic Devices and Systems of the Ministry of Education and Guangdong Province, College of Physics and Optoelectronic Engineering, Shenzhen University, Shenzhen 518060, P. R. China*

Zuqing Yuan − *CAS Center for Excellence in Nanoscience, Beijing Key Laboratory of Micro-Nano Energy and Sensor, Beijing Institute of Nanoenergy and Nanosystems, Chinese Academy of Sciences, Beijing 101400, P. R. China;* orcid.org/0000-0003-3988-0618

Ping Chen − *Center on Nanoenergy Research, School of Physical Science and Technology, Guangxi University, Nanning, Guangxi 530004, P. R. China*

Dengfeng Peng − *Key Laboratory of Optoelectronic Devices and Systems of the Ministry of Education and Guangdong Province, College of Physics and Optoelectronic Engineering, Shenzhen University, Shenzhen 518060, P. R. China*

Complete contact information is available at: https://pubs.acs.org/10.1021/acsnano.1c09779

Notes

The authors declare no competing financial interest.

ACKNOWLEDGMENTS

The authors are thankful for the support from the National Natural Science Foundation of China (52125205, U20A20166, 61805015, 52002246, 61875136, and 61804011), the Shenzhen Fundamental Research Project (JCYJ20190808170601664), the Science and Technology Innovation Project of Shenzhen Excellent Talents (RCBS20200714114919006), the Natural Science Foundation of Beijing Municipality (Z180011), the Fundamental Research Project of Guangdong Province (2020A1515011315), the Shenzhen Science and Technology Program (KQTD20170810105439418), and the Fundamental Research Funds for the Central Universities.

REFERENCES

(1) Jung, D.; Lim, C.; Shim, H. J.; Kim, Y.; Park, C.; Jung, J.; Han, S. I.; Sunwoo, S.-H.; Cho, K. W.; Cha, G. D.; Kim, D. C.; Koo, J. H.; Kim, J. H.; Hyeon, T.; Kim, D.-H. Highly Conductive and Elastic Nanomembrane for Skin Electronics. *Science* **2021**, *373* (6558), 1022−1026.

(2) Shih, B.; Shah, D.; Li, J.; Thuruthel, T. G.; Park, Y.-L.; Iida, F.; Bao, Z.; Kramer-Bottiglio, R.; Tolley, M. T. Electronic Skins and Machine Learning for Intelligent Soft Robots. *Sci. Robot.* **2020**, *5* (41), No. eaaz9239.

(3) Lee, Y.; Park, J.; Choe, A.; Cho, S.; Kim, J.; Ko, H. Mimicking Human and Biological Skins for Multifunctional Skin Electronics. *Adv. Funct. Mater.* **2020**, *30* (20), 1904523.

(4) Wang, C.; Pan, C.; Wang, Z. Electronic Skin for Closed-Loop Systems. *ACS Nano* **2019**, *13* (11), 12287−12293.

(5) Liu, H.; Chen, X.; Zheng, Y.; Zhang, D.; Zhao, Y.; Wang, C.; Pan, C.; Liu, C.; Shen, C. Lightweight, Superelastic and Hydrophobic Polyimide Nanofiber /MXene Composite Aerogel for Wearable Piezoresistive Sensor and Oil/Water Separation Applications. *Adv. Funct. Mater.* **2021**, *31* (13), 2008006.

(6) Zhou, K.; Zhao, Y.; Sun, X.; Yuan, Z.; Zheng, G.; Dai, K.; Mi, L.; Pan, C.; Liu, C.; Shen, C. Ultra-Stretchable Triboelectric Nanogenerator as High-Sensitive and Self-Powered Electronic Skins for Energy Harvesting and Tactile Sensing. *Nano Energy* **2020**, *70*, 104546.

(7) Liu, H.; Li, Q.; Bu, Y.; Zhang, N.; Wang, C.; Pan, C.; Mi, L.; Guo, Z.; Liu, C.; Shen, C. Stretchable Conductive Nonwoven Fabrics with Self-Cleaning Capability for Tunable Wearable Strain Sensor. *Nano Energy* **2019**, *66*, 104143.

(8) Zhou, K.; Xu, W.; Yu, Y.; Zhai, W.; Yuan, Z.; Dai, K.; Zheng, G.; Mi, L.; Pan, C.; Liu, C.; Shen, C. Tunable and Nacre-Mimetic Multifunctional Electronic Skins for Highly Stretchable Contact-Noncontact Sensing. *Small* **2021**, *17* (31), 2100542.
(9) Li, E.; Pan, Y.; Wang, C.; Liu, C.; Shen, C.; Pan, C.; Liu, X. Asymmetric Superhydrophobic Textiles for Electromagnetic Interference Shielding, Photothermal Conversion and Solar Water Evaporation. *ACS Appl. Mater. Interfaces* **2021**, *13* (24), 28996−29007.
(10) Li, E.; Pan, Y.; Wang, C.; Liu, C.; Shen, C.; Pan, C.; Liu, X. Multifunctional and Superhydrophobic Cellulose Composite Paper for Electromagnetic Shielding, Hydraulic Triboelectric Nanogenerator and Joule Heating Applications. *Chem. Eng. J.* **2021**, *420*, 129864.
(11) Han, X.; Xu, Z.; Wu, W.; Liu, X.; Yan, P.; Pan, C. Recent Progress in Optoelectronic Synapses for Artificial Visual-Perception System. *Small Struct.* **2020**, *1* (3), 2000029.
(12) Li, S.; Zhang, Y.; Wang, Y.; Xia, K.; Yin, Z.; Wang, H.; Zhang, M.; Liang, X.; Lu, H.; Zhu, M.; Wang, H.; Shen, X.; Zhang, Y. Physical Sensors for Skin-Inspired Electronics. *InfoMater.* **2020**, *2* (1), 184−211.
(13) Jiang, X.-Z.; Sun, Y.-J.; Fan, Z.; Zhang, T.-Y. Integrated Flexible, Waterproof, Transparent and Self-Powered Tactile Sensing Panel. *ACS Nano* **2016**, *10* (8), 7696−7704.
(14) Haque, R. I.; Chandran, O.; Lani, S.; Briand, D. Self-Powered Triboelectric Touch Sensor Made of 3D Printed Materials. *Nano Energy* **2018**, *52*, 54−62.
(15) Wu, X.; Zhu, J.; Evans, J. W.; Lu, C.; Arias, A. C. A Potentiometric Electronic Skin for Thermosensation and Mechanosensation. *Adv. Funct. Mater.* **2021**, *31* (17), 2010824.
(16) Li, G.; Liu, S.; Wang, L.; Zhu, R. Skin-Inspired Quadruple Tactile Sensors Integrated on a Robot Hand Enable Object Recognition. *Sci. Robot.* **2020**, *5* (49), No. eabc8134.
(17) Kwak, J. W.; Han, M.; Xie, Z.; Chung, H. U.; Lee, J. Y.; Avila, R.; Yohay, J.; Chen, X.; Liang, C.; Patel, M.; Jung, I.; Kim, J.; Namkoong, M.; Kwon, K.; Guo, X.; Ogle, C.; Grande, D.; Ryu, D.; Kim, D. H.; Madhvapathy, S.; et al. Wireless Sensors for Continuous, Multimodal Measurements at the Skin Interface with Lower Limb Prostheses. *Sci. Transl. Med.* **2020**, *12* (574), No. eabc4327.
(18) Zhang, Z.; Chen, Z.; Wang, Y.; Zhao, Y. Bioinspired Conductive Cellulose Liquid-Crystal Hydrogels as Multifunctional Electrical Skins. *Proc. Natl. Acad. Sci. U. S. A.* **2020**, *117* (31), 18310−18316.
(19) Jin, W.; Kim, E. H.; Lee, S.; Yu, S.; Han, H.; Kim, G.; Lee, S. W.; Jang, J.; Lee, C. E.; Shim, W.; Park, C. Tandem Interactive Sensing Display De-Convoluting Dynamic Pressure and Temperature. *Adv. Funct. Mater.* **2021**, *31* (23), 2010492.
(20) Peng, Y.; Lu, J.; Peng, D.; Ma, W.; Li, F.; Chen, Q.; Wang, X.; Sun, J.; Liu, H.; Pan, C. Dynamically Modulated GaN Whispering Gallery Lasing Mode for Strain Sensor. *Adv. Funct. Mater.* **2019**, *29* (42), 1905051.
(21) Wang, C.; Zhao, J.; Ma, C.; Sun, J.; Tian, L.; Li, X.; Li, F.; Han, X.; Liu, C.; Shen, C.; Dong, L.; Yang, J.; Pan, C. Detection of Non-Joint Areas Tiny Strain and Anti-Interference Voice Recognition by Micro-Cracked Metal Thin Film. *Nano Energy* **2017**, *34*, 578−585.
(22) Zhang, H.; Peng, D.; Wang, W.; Dong, L.; Pan, C. Mechanically Induced Light Emission and Infrared-Laser-Induced Upconversion in the Er-Doped CaZnOS Multifunctional Piezoelectric Semiconductor for Optical Pressure and Temperature Sensing. *J. Phys. Chem. C* **2015**, *119* (50), 28136−28142.
(23) Ruth, S. R. A.; Feig, V. R.; Kim, M.-G.; Khan, Y.; Phong, J. K.; Bao, Z. Flexible Fringe Effect Capacitive Sensors with Simultaneous High-Performance Contact and Non-Contact Sensing Capabilities. *Small Struct.* **2021**, *2* (2), 2000079.
(24) Chen, C.; Zhuang, Y.; Li, X.; Lin, F.; Peng, D.; Tu, D.; Xie, A.; Xie, R.-J. Achieving Remote Stress and Temperature Dual-Modal Imaging by Double-Lanthanide-Activated Mechanoluminescent Materials. *Adv. Funct. Mater.* **2021**, *31* (25), 2101567.
(25) Zhang, Q.; Zuo, S.; Chen, P.; Pan, C. Piezotronics in Two-Dimensional Materials. *InfoMater.* **2021**, *3* (9), 987−1007.
(26) Someya, T.; Kato, Y.; Sekitani, T.; Iba, S.; Noguchi, Y.; Murase, Y.; Kawaguchi, H.; Sakurai, T. Conformable, Flexible, Large-Area Networks of Pressure and Thermal Sensors with Organic Transistor Active Matrixes. *Proc. Natl. Acad. Sci. U. S. A.* **2005**, *102* (35), 12321−12325.
(27) Tien, N. T.; Jeon, S.; Kim, D.-I.; Trung, T. Q.; Jang, M.; Hwang, B.-U.; Byun, K.-E.; Bae, J.; Lee, E.; Tok, J. B.-H.; Bao, Z.; Lee, N.-E.; Park, J.-J. A Flexible Bimodal Sensor Array for Simultaneous Sensing of Pressure and Temperature. *Adv. Mater.* **2014**, *26* (5), 796−804.
(28) Zhang, F.; Zang, Y.; Huang, D.; Di, C.-A.; Zhu, D. Flexible and Self-Powered Temperature-Pressure Dual-Parameter Sensors Using Microstructure-Frame-Supported Organic Thermoelectric Materials. *Nat. Commun.* **2015**, *6* (1), 8356.
(29) Ye, C.; Ren, J.; Wang, Y.; Zhang, W.; Qian, C.; Han, J.; Zhang, C.; Jin, K.; Buehler, M. J.; Kaplan, D. L.; Ling, S. Design and Fabrication of Silk Templated Electronic Yarns and Applications in Multifunctional Textiles. *Matter* **2019**, *1* (5), 1411−1425.
(30) Lu, L.; Yang, B.; Liu, J. Flexible Multifunctional Graphite Nanosheet/Electrospun-Polyamide 66 Nanocomposite Sensor for ECG, Strain, Temperature and Gas Measurements. *Chem. Eng. J.* **2020**, *400*, 125928.
(31) Wang, Y.; Wu, H.; Xu, L.; Zhang, H.; Yang, Y.; Wang, Z. L. Hierarchically Patterned Self-Powered Sensors for Multifunctional Tactile Sensing. *Sci. Adv.* **2020**, *6* (34), No. eabb9083.
(32) Sun, Q.-J.; Zhao, X.-H.; Zhou, Y.; Yeung, C.-C.; Wu, W.; Venkatesh, S.; Xu, Z.-X.; Wylie, J. J.; Li, W.-J.; Roy, V. A. L. Fingertip-Skin-Inspired Highly Sensitive and Multifunctional Sensor with Hierarchically Structured Conductive Graphite/Polydimethylsiloxane Foams. *Adv. Funct. Mater.* **2019**, *29* (18), 1808829.
(33) Zhao, X.-H.; Ma, S.-N.; Long, H.; Yuan, H.; Tang, C. Y.; Cheng, P. K.; Tsang, Y. H. Multifunctional Sensor Based on Porous Carbon Derived from Metal-Organic Frameworks for Real Time Health Monitoring. *ACS Appl. Mater. Interfaces* **2018**, *10* (4), 3986−3993.
(34) Park, H.; Kim, J. W.; Hong, S. Y.; Lee, G.; Kim, D. S.; Oh, J. H.; Jin, S. W.; Jeong, Y. R.; Oh, S. Y.; Yun, J. Y.; Ha, J. S. Microporous Polypyrrole-Coated Graphene Foam for High-Performance Multifunctional Sensors and Flexible Supercapacitors. *Adv. Funct. Mater.* **2018**, *28* (33), 1707013.
(35) Bae, G. Y.; Han, J. T.; Lee, G.; Lee, S.; Kim, S. W.; Park, S.; Kwon, J.; Jung, S.; Cho, K. Pressure/Temperature Sensing Bimodal Electronic Skin with Stimulus Discriminability and Linear Sensitivity. *Adv. Mater.* **2018**, *30* (43), 1803388.
(36) Bing, W.; Wang, H.; Tian, L.; Zhao, J.; Jin, H.; Du, W.; Ren, L. Small Structure, Large Effect: Functional Surfaces Inspired by Salvinia Leaves. *Small Struct.* **2021**, *2* (9), 2100079.
(37) Das, C. M.; Kang, L.; Ouyang, Q.; Yong, K.-T. Advanced Low-Dimensional Carbon Materials for Flexible Devices. *InfoMater.* **2020**, *2* (4), 698−714.
(38) An, B. W.; Heo, S.; Ji, S.; Bien, F.; Park, J.-U. Transparent and Flexible Fingerprint Sensor Array with Multiplexed Detection of Tactile Pressure and Skin Temperature. *Nat. Commun.* **2018**, *9* (1), 2458.
(39) Walia, S.; Mondal, I.; Kulkarni, G. U. Patterned Cu-Mesh-Based Transparent and Wearable Touch Panel for Tactile, Proximity, Pressure and Temperature Sensing. *ACS Appl. Electron. Mater.* **2019**, *1* (8), 1597−1604.
(40) Song, K.; Zhao, R.; Wang, Z. L.; Yang, Y. Conjuncted Pyro-Piezoelectric Effect for Self-Powered Simultaneous Temperature and Pressure Sensing. *Adv. Mater.* **2019**, *31* (36), 1902831.
(41) Park, J.; Kim, M.; Lee, Y.; Lee, H. S.; Ko, H. Fingertip Skin-Inspired Microstructured Ferroelectric Skins Discriminate Static/Dynamic Pressure and Temperature Stimuli. *Sci. Adv.* **2015**, *1* (9), No. e1500661.
(42) Zhu, M.; Zhang, F.; Chen, X. Bioinspired Mechanically Interlocking Structures. *Small Struct.* **2020**, *1* (3), 2000045.

https://doi.org/10.1021/acsnano.1c09779
ACS Nano 2022, 16, 2789−2797

(43) Ge, G.; Lu, Y.; Qu, X.; Zhao, W.; Ren, Y.; Wang, W.; Wang, Q.; Huang, W.; Dong, X. Muscle-Inspired Self-Healing Hydrogels for Strain and Temperature Sensor. *ACS Nano* **2020**, *14* (1), 218−228.
(44) Gu, J.; Huang, J.; Chen, G.; Hou, L.; Zhang, J.; Zhang, X.; Yang, X.; Guan, L.; Jiang, X.; Liu, H. Multifunctional Poly(vinyl alcohol) Nanocomposite Organohydrogel for Flexible Strain and Temperature Sensor. *ACS Appl. Mater. Interfaces* **2020**, *12* (36), 40815−40827.
(45) Hua, Q.; Sun, J.; Liu, H.; Bao, R.; Yu, R.; Zhai, J.; Pan, C.; Wang, Z. L. Skin-Inspired Highly Stretchable and Conformable Matrix Networks for Multifunctional Sensing. *Nat. Commun.* **2018**, *9* (1), 244.
(46) You, I.; Mackanic, D. G.; Matsuhisa, N.; Kang, J.; Kwon, J.; Beker, L.; Mun, J.; Suh, W.; Kim, T. Y.; Tok, J. B.-H.; Bao, Z.; Jeong, U. Artificial Multimodal Receptors Based on Ion Relaxation Dynamics. *Science* **2020**, *370* (6519), 961−965.
(47) Wang, C.; Peng, D.; Pan, C. Mechanoluminescence Materials for Advanced Artificial Skin. *Sci. Bull.* **2020**, *65* (14), 1147−1149.
(48) Zhuang, Y.; Xie, R.-J. Mechanoluminescence Rebrightening the Prospects of Stress Sensing: a Review. *Adv. Mater.* **2021**, *33*, 2005925.
(49) Zhao, Y.; Peng, D.; Bai, G.; Huang, Y.; Xu, S.; Hao, J. Multiresponsive Emissions in Luminescent Ions Doped Quaternary Piezophotonic Materials for Mechanical-to-Optical Energy Conversion and Sensing Applications. *Adv. Funct. Mater.* **2021**, *31*, 2010265.
(50) Wang, X.; Zhang, H.; Yu, R.; Dong, L.; Peng, D.; Zhang, A.; Zhang, Y.; Liu, H.; Pan, C.; Wang, Z. L. Dynamic Pressure Mapping of Personalized Handwriting by a Flexible Sensor Matrix Based on the Mechanoluminescence Process. *Adv. Mater.* **2015**, *27* (14), 2324−2331.
(51) Wang, C.; Ma, R.; Peng, D.; Liu, X.; Li, J.; Jin, B.; Shan, A.; Fu, Y.; Dong, L.; Gao, W.; Wang, Z. L.; Pan, C. Mechanoluminescent Hybrids from a Natural Resource for Energy-Related Applications. *InfoMater.* **2021**, *3* (11), 1272−1284.
(52) Lou, Z.; Shen, G. Flexible Image Sensors with Semiconducting Nanowires for Biomimic Visual Applications. *Small Struct.* **2021**, *2* (7), 2000152.
(53) Bao, R.; Tao, J.; Pan, C.; Wang, Z. L. Piezophototronic Effect in Nanosensors. *Small Sci.* **2021**, *1* (6), 2000060.
(54) Wang, X.; Zhou, H.; Yuan, S.; Zheng, W.; Jiang, Y.; Zhuang, X.; Liu, H.; Zhang, Q.; Zhu, X.; Wang, X.; Pan, A. Cesium Lead Halide Perovskite Triangular Nanorods as High-Gain Medium and Effective Cavities for Multiphoton-Pumped Lasing. *Nano Res.* **2017**, *10* (10), 3385−3395.
(55) Peng, D.; Jiang, Y.; Huang, B.; Du, Y.; Zhao, J.; Zhang, X.; Ma, R.; Golovynskyi, S.; Chen, B.; Wang, F. A ZnS/CaZnOS Heterojunction for Efficient Mechanical-to-Optical Energy Conversion by Conduction Band Offset. *Adv. Mater.* **2020**, *32* (16), 1907747.
(56) Zhang, Y.; Cui, Y. Development of Flexible and Wearable Temperature Sensors Based on PEDOT:PSS. *IEEE Trans. Electron Devices* **2019**, *66* (7), 3129−3133.

https://doi.org/10.1021/acsnano.1c09779
ACS Nano 2022, 16, 2789−2797